Zigzag edge ferromagnetism of triangular-graphene-quantum-dot-like system

Runze Han,[1] Jiazhou Chen,[1] Mengyue Zhang,[1] Jinze Gao,[1] Yicheng Xiong,[1] Yue Pan,[1,*] and Tianxing Ma[1,2,†]
[1]*Department of Physics, Beijing Normal University, Beijing 100875, China*
[2]*Key Laboratory of Multiscale Spin Physics (Ministry of Education), Beijing Normal University, Beijing 100875, China*

(Received 2 May 2023; revised 18 January 2024; accepted 23 January 2024; published 9 February 2024)

Here, the magnetic susceptibility of a triangular-graphene-quantum-dot-like system was examined by using the determinant quantum Monte Carlo method. We focused on three zigzag edge quantum dots or rings, namely, the triangular graphene quantum ring, bilayer triangular graphene quantum dots, and bilayer triangular graphene quantum ring. The triangular-graphene-quantum-dot-like system exhibited robust edge ferromagnetic behavior, which was independent of size, monolayer or bilayer, or dot or ring shape, according to the numerical results. At half filling, the edge magnetic susceptibility is increased by on-site interactions, especially in the low-temperature region. Spintronics systems may benefit from use of this system due to its robust edge ferromagnetic behavior.

DOI: 10.1103/PhysRevB.109.075117

I. INTRODUCTION

The rich physical features of graphene have led to its extensive research and application development in the domains of electrical [1–4], optics [5,6], and other fields over the past few decades. Numerous research groups have explored the properties which were effected by the stacking mode in multilayer graphene [7–18]. Additionally, with the increasing demand for low-power devices, the field of spintronics is rapidly developing, and novel magnetic properties have also been found in both monolayer and bilayer graphene. Therefore, the investigation into the possible ferromagnetism of graphene is significant for expanding its use in spintronic applications.

The electronic and magnetic properties of various graphene systems are significantly influenced by their edge atomic configurations [19–23], such as armchair or zigzag types. Zigzag-edge graphene exhibits magnetism due to ferromagnetic coupling along each zigzag edge and antiferromagnetic coupling between two parallel zigzag edges. The presence of strong ferromagnetic coupling along zigzag edges has been theoretically predicted [24–26] and verified by experiments [27–29]. The disruption of sublattice symmetry by zigzag edges is a primary factor contributing to graphene's magnetism [30]. Furthermore, experimental studies have observed spin-related phenomena to arise from zigzag edges in graphene [31,32]. Since zigzag edges as effective strategies have been attempted to realize ferromagnetic ordering, graphene nanoribbons (GNRs) [33–35] and graphene quantum dots (GQDs) [36–38] have received increasing attention. Both of these can be thought of as putting constraints on an endlessly long two-dimensional lattice, and the edge region itself shows a variety of magnetic phenomena. GNRs allow for infinite extension in one direction while being finite in another. However, GQDs are nanometric in all dimensions and display remarkable optoelectronic properties due to quantum confinement and edge effects, as compared to other quantum dots [38]. Theoretical approaches, like quantum Monte Carlo (QMC) method and density functional theory (DFT) simulations [37,38], have predicted strong edge magnetism even in GQDs. Recent advancements in fabrication techniques have promoted the precise creation of GQDs with varied shapes and sizes, offering a unique opportunity to investigate the impact of zigzag edges on GQDs' magnetic properties.

Among various graphene quantum dot structures, triangular-graphene-quantum-dot-like (TGQD-like) systems stand out, including triangular graphene quantum dots (TGQDs) [39,40], bilayer TGQDs [41], triangular graphene quantum rings (TGQRs) [42,43], and bilayer TGQRs [44]. Although the magnetic properties of TGQDs consistent with Lieb's theorem where boundary conditions influence energy spectra in finite-sized systems, magnetic fields do not impact edge states [45–48]. Moreover, experimental efforts have significantly advanced in probing the frontier molecular orbitals of TGQDs [49–52]. As we all know, stacking layers of graphene can have a significant impact on its magnetic properties. The electronic and transport properties of bilayer graphene quantum dots has also been recently reported [53–56]. However, the geometry of TGQD-like systems make such systems harder to be studied by analytical methods, necessitating the use of numerically exact methods for investigating TGQDs and TGQRs with zigzag edges.

In this work, we will further provide numerical simulations on the magnetism of the Hubbard model in TGQD-like systems using the determinant quantum Monte Carlo (DQMC) method. We observe that the edge magnetic susceptibility of three types of quantum dots (rings) at finite temperatures exhibits Curie-Weiss behavior, indicating the edge ferromagnetism's robustness in TGQD-like systems, regardless of size, layering, and shape. Notably, at low temperatures, the edge magnetic susceptibility increases with the on-site Hubbard interaction near the half-filling state. This robust edge

*pany@mail.bnu.edu.cn
†txma@bnu.edu.cn

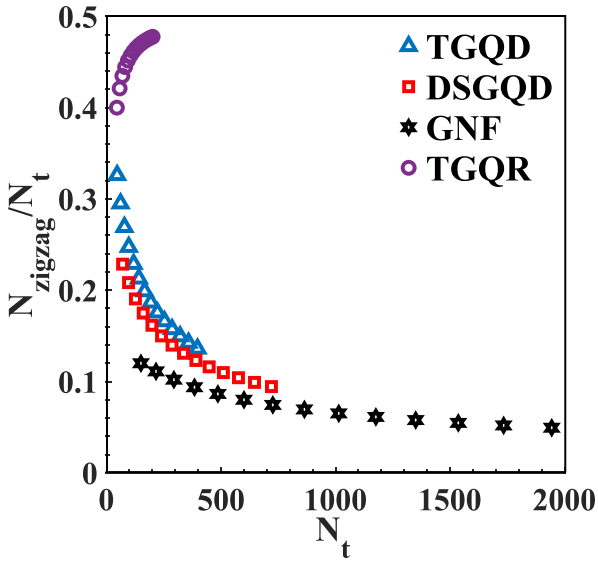

FIG. 1. The relationship between the ratio of the number of atoms at zigzag edge to total number of atoms N_{zigzag}/N_t and N_t of TGQD, diamond shaped GQD (DSGQD), graphene nanoflake (GNF), TGQR, respectively.

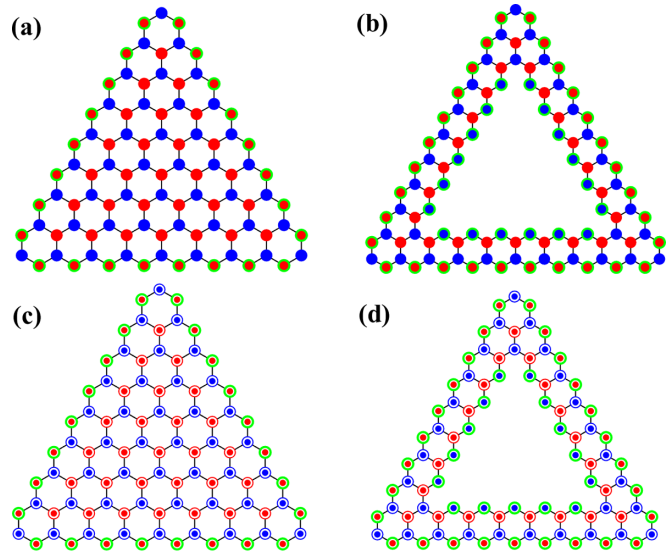

FIG. 2. Sketches for (a) a TGQD with 97 sites, (b) a TGQR with 105 sites, (c) a bilayer TGQD with 92 sites, and (d) a bilayer TGQR with 114 sites. In the subgraph (a) and (b), blue and red solid circles indicate A and B sublattices, respectively. In the subgraph (c) and (d), red and blue solid circles indicate A and B sublattices of the bottom layer, while red and blue hollow circles indicate sublattices of the top layer, respectively. The sites at the zigzag edge are marked by green marker edge.

ferromagnetic behavior holds potential implications for spintronic applications.

II. MODEL AND METHODS

We select the quantum dot model that most accurately captures the zigzag edge circumstances because the zigzag edge of graphene is more prone to ferromagnetism. We determined that the total number of atoms N_t varies with the percentage N_{zigzag}/N_t of graphene nanoflakes, diamond-shaped GQDs, TGQDs, and TGQRs with zigzag edges at different lattice sites, as shown in Fig. 1.

It is apparent that the ratio of edge atoms in quantum rings is greater than that in bulk quantum dots, as shown in Fig 1. There are significantly fewer nonedge sites in the configuration of quantum rings than in quantum dots, and there is an inner edge in quantum rings. The edge proportion of the TGQD is the highest of the three common quantum dots. Similarly, TGQR was studied because of its high proportion of edge regions compared to the total area. We shall investigate only TGQRs with a hexagonal lattice of ring width, that is, the difference between the outer diameter and inner diameter of TGQRs in units of the graphene hexagonal lattice width. The potential differences in edge magnetism between quantum rings and quantum dots were also examined. As the ring width narrows, the ratio of edge atoms to the overall number of atoms increases.

In Fig. 2(a), the TGQD sketch is presented, while Figs. 2(b)–2(d) depict the TGQR, bilayer TGQD, and bilayer TGQR sketches. In particular, solid circles stand for the sites of the top layer in the bilayer TGQD and the bilayer TGQR, and the hollow circles represent the bottom layer. A, B sublattices are distinguished by different colors, and the sites at the zigzag edge are highlighted by green marker edge. The Hamiltonian of TGQD-like system is expressed as follows:

$$H = H_k + H_k' + H_\mu + H_U. \tag{1}$$

Among them,

$$H_k = -t \sum_{l\langle i,j\rangle\sigma} (a^\dagger_{li\sigma} b_{lj\sigma} + \text{H.c.}), \tag{2}$$

$$H_k' = -\sum_{i,j,l\neq l',\sigma} t_{ij} (a^\dagger_{li\sigma} a_{l'j\sigma} + a^\dagger_{li\sigma} b_{l'j\sigma} + b^\dagger_{li\sigma} a_{l'j\sigma} + b^\dagger_{li\sigma} b_{l'j\sigma}), \tag{3}$$

$$H_\mu = \mu \sum_{i,l,\sigma} (n_{lai\sigma} + n_{lbi\sigma}), \tag{4}$$

$$H_U = U \sum_{i,l} (n_{lai\uparrow} n_{lai\downarrow} + n_{lbi\uparrow} n_{lbi\downarrow}). \tag{5}$$

H_k is the intralayer hopping term, and H_k' is the interlayer hopping term, which is zero for monolayer graphene. H_μ represents the chemical potential and H_U represents the on-site Hubbard interaction. i and j represent different lattice site index, and $\langle i, j\rangle$ represents a pair of nearest neighbors (NN). $a^\dagger_{li\sigma}(a_{li\sigma})$ creates (annihilates) electrons with spin $\sigma(\sigma = \uparrow, \downarrow)$ at the i lattice point on sublattice A of the l layer, as well as $b^\dagger_{li\sigma}(b_{li\sigma})$ acting on electrons of sublattice B. $n_{lai\sigma} = a^\dagger_{li\sigma} a_{li\sigma}$ and $n_{lbi\sigma} = b^\dagger_{li\sigma} b_{li\sigma}$. $t = 2.7$ eV is the NN hopping integral, which is a typical value that best reproduces the slopes of the valence and conduction bands at the K point from DFT calculations and is consistent with the experimental parameters [2,57,58]. t_{ij} is the hopping integral from lattice site $\boldsymbol{R_{1i}}$

of one layer to lattice site $\boldsymbol{R_{2j}}$ of the other layer, satisfying

$$t_{ij} = t_c e^{-(|\boldsymbol{R}_{1i}^{d} - \boldsymbol{R}_{2j}^{d'}| - d_0)/\xi}. \tag{6}$$

For $t_c = 0.17t$, the vertical distance is $d_0 = 0.335$ nm, and $\xi = 0.0453$ nm [59]. It indicates the interlayer hopping from $\boldsymbol{R_{1i}}$ of the first layer to $\boldsymbol{R_{2j}}$ of the second layer, which is related to the relative position of the two lattices $|\boldsymbol{R_{1i}}^{d} - \boldsymbol{R_{2j}}^{d'}|$. t_{ij} decreases exponentially with interlayer distance and becomes negligible beyond $3.0a$. A two-center Slater-Koster type model can be used to describe the p_z orbitals on carbon atoms. The hopping terms are shown below [60,61]:

$$t(\boldsymbol{r}) = V_{pp\pi}(\boldsymbol{r}) + V_{pp\sigma}(\boldsymbol{r}), \tag{7}$$

where

$$V_{pp\pi}(\boldsymbol{r}) = t_{pp\pi} e^{-(|\boldsymbol{R}_{1i}^{d} - \boldsymbol{R}_{2j}^{d'}| - d_0)/\xi} \tag{8}$$

and

$$V_{pp\sigma}(\boldsymbol{r}) = t_{pp\sigma} e^{-(|\boldsymbol{R}_{1i}^{d} - \boldsymbol{R}_{2j}^{d'}| - d_0)/\xi} \left(\frac{\boldsymbol{r}\cdot\boldsymbol{e}_z}{|\boldsymbol{r}|}\right)^2. \tag{9}$$

For Eq. (6), the parameter t corresponds to the $pp\sigma$ term of the Slater-Koster hopping parameters, whereas t_c is associated with the $pp\pi$ term [62].

We probe the edge magnetic properties of three different types of quantum dots (rings) at finite temperature using DQMC simulations. In this method, the action $e^{-\beta H}$ is split into M slices by Trotter decomposition, namely $e^{-\beta H} = \prod_M e^{-\Delta\tau H}$. Then, the interaction term is decoupled by using Hubbard-Stratonovich transformation [63,64]. These observations can be reproduced in calculation using a particular auxiliary field configuration because the action will be bilinear after transformation. In practice, the target observations are obtained by sampling in the configuration space. The simulation provides 8000 warm-up sweeps to equilibrate the system, and 30 000 sweeps were subsequently conducted for the measurements. The number of measurements was split into ten bins, which provide the basis for coarse-grain averages and errors estimated based on standard deviations from the averages so that the simulation can be performed at low enough temperatures to converge to the ground state. At half filling, the particle-hole symmetry frees our system from the sign problem.

The uncertainty of the Coulomb interaction parameter U in graphene and its derivatives is noteworthy. This value can be inferred from estimations made for polyacetylene [2,65,66], where U ranges between 6.0 eV and 17.0 eV, encompassing a broad range of values. To examine the influence of interactions on magnetic properties in such systems, our simulations consider U values from $1.0|t|$ to $4.0|t|$. In the remainder of this paper, we set t as the unit.

III. RESULTS

We introduce χ_b and χ_z to describe the magnetic susceptibility of the bulk quantum dot (ring) and the zigzag edge, respectively, in order to characterize the ferromagnetic behavior of the system [67],

$$\chi = \int_0^\beta d\tau \sum_{d,d'=a,b} \sum_{i,j} \langle m_{i_d}(\tau)\cdot m_{j_{d'}}(0)\rangle, \tag{10}$$

where $m_{i_a}(\tau) = e^{H\tau} m_{i_a}(0) e^{-H\tau}$, $m_{i_a} = a_{i\uparrow}^{\dagger} a_{i\uparrow} - a_{i\downarrow}^{\dagger} a_{i\downarrow}$, and sublattices A and B are equivalent. The bulk magnetic susceptibility χ_b is the average of the zz spin correlation of all sublattices, and χ_z is the average of the sublattice of the zigzag edge of the quantum dot (ring), which is shown in Fig. 2 with special marking edges.

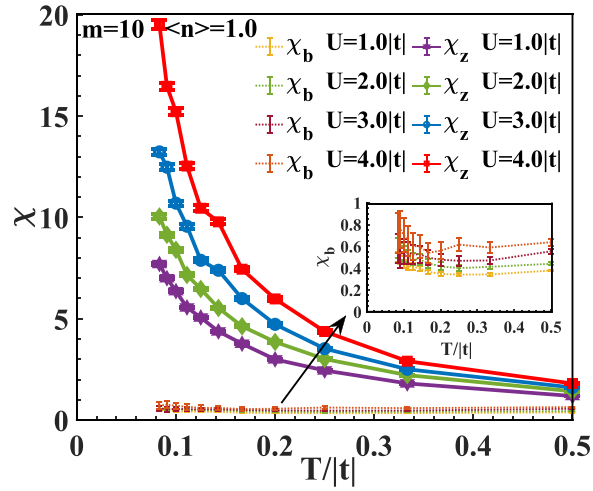

FIG. 3. The χ_z (solid line) and χ_b (dotted line) of a TGQR at $\langle n\rangle = 1.0$ with different U, and m in the tag represents the number of hexagons contained by the edge of the triangle ring.

To determine how the edge magnetic susceptibility of TGQRs changes with temperature at various on-site interactions $U = 1.0|t| \sim 4.0|t|$, we first plot Fig. 3 and that χ_z decreases with temperature in an inversely proportional way. We assume that the edge of the TGQR is ferromagnetic according to the Curie-Weiss law $\chi = C/(T - T_C)$. The law shows the connection between magnetic susceptibility and temperature in ferromagnetic materials below the Curie temperature T_C.

We choose two values of U for fitting. The first typical U is derived from the Peierls-Feynman-Bogoliubov variational principle, which maps a generalized Hubbard model with nonlocal Coulomb interactions onto an effective Hubbard model with only on-site effective interactions U, demonstrating that U is approximately $1.6|t|$ [68]. The second one, $U = 3.0|t|$ [67], is a typical value for examining how interactions affect the magnetic characteristics of quantum dots. For these calculations, we use the following formula:

$$\chi = \frac{C}{T - T_C}. \tag{11}$$

According to Fig. 4, TGQR exhibits conventional ferromagnetic behavior, and the relationship between χ_z and temperature satisfies the Curie-Weiss law. The T_C is approximately $0.033|t|$ at $U = 3.0|t|$ and approximately $0.013|t|$ at $U = 1.6|t|$.

The Monte Carlo approach results in larger intrinsic variances due to the process of sampling at lower temperatures,

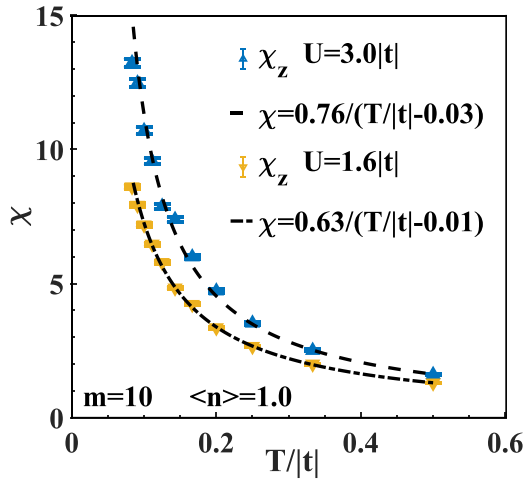

FIG. 4. The χ_z of a TGQR of $m = 10$ at $\langle n\rangle = 1.0$ with $U = 1.6|t|$ and $3.0|t|$ and the fitting of Curie's law, respectively.

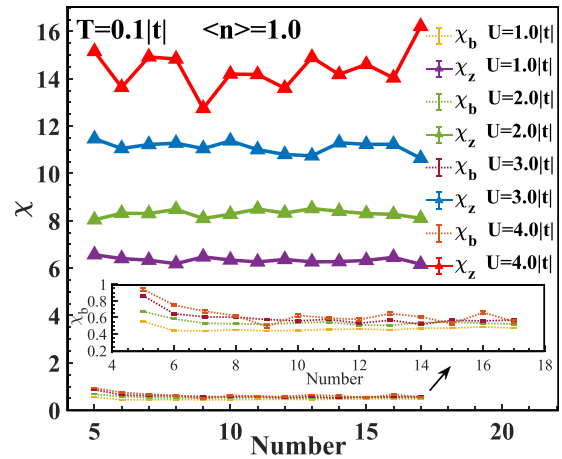

FIG. 5. The χ_z (solid line) and χ_b (dotted line) of TGQR of different size at $\langle n\rangle = 1.0$ with different U. "Number" represents for the number of hexagons contained by the edge of the triangle ring.

which produces a slightly incorrect result. The magnetic susceptibility at the lowest temperature in the calculation result is used to estimate the maximum inaccuracy of T_C,

$$\delta T_C = \frac{C}{\chi^2}\delta\chi. \tag{12}$$

For $U = 3.0|t|$, δT_C is approximately $0.008|t|$. For $U = 1.6|t|$, δT_C is approximately $0.005|t|$. Our results demonstrate the edge ferromagnetic feature even when the interaction U is small.

The bulk magnetic susceptibility χ_b is flat and can be deduced from the half-filled Hubbard model on the ideal honeycomb lattice due to its antiferromagnetism in the ground state.

For any central atom, the NN atom has a negative spin correlation factor because the hexagonal honeycomb lattice is antiferromagnetic. This spin correlation between the next-nearest neighbor (NNN) atom and the central atom is positive, that is, ferromagnetic correlation, because the NNN atom and NN atom have a NN relationship. The center atom and the NNN atom are connected by a NN relationship to the same sublattice, according to the graphene structure. Therein, the high dependence of χ_z on temperature may be caused by the fact that the atoms at the zigzag edges belong to the same sublattice.

We show χ_b and χ_z as the number of hexagonal lattices at the TGQR edge shifts from 5 to 17 under the conditions of $T = 0.1|t|$ and $\langle n\rangle = 1.0$ to investigate the impact of the size effect on TGQR edge ferromagnetism, as shown in Fig. 5. With an increase in the quantum ring size, χ_b and χ_z gradually change. The magnetic susceptibility scarcely changes with structure size, especially at low U ($U = 3.0|t|$ and below), suggesting that the robustness of TGQR with zigzag edges is unaffected by size. This phenomenon occurs because the TGQR edge structure is a typical zigzag structure and has a significant ferromagnetic correlation. In addition, we deduce that a larger on-site interaction U can greatly increase the Curie temperature of the system by enhancing the magnetic susceptibility of the edge.

Starting with the smallest TGQR, each side of the triangle contains five honeycomb lattices, that is, five zigzag edge atoms. In this case, the ferromagnetic correlation of its edge has been saturated, signifying that the spins of the electrons on the edge are practically in the same direction. As a result, adding more atoms with zigzag edges will not strengthen the ferromagnetic correlation. A change in system size may result in an erratic oscillation of the edge magnetic susceptibility at higher U. At the same temperature, we also observe from Figs. 3 and 5 that χ_b and χ_z increase as U increases. Figure 4 indicates that as U increases, the Curie temperature increases.

We estimated the changes in magnetic susceptibility of TGQD and TGQR bilayers with temperature and size to investigate the impact of interlayer coupling on the edge magnetism. The DQMC can be applied to approximately 100 quantum dot (ring) lattice sites with precise sampling and calculation of physical quantities, and the result is shown in Fig. 6. In the half-filled system, the χ_z and χ_b of the bilayer TGQD and the bilayer TGQR increase with increasing U, and χ_z dramatically decreases with increasing T; however, the change in χ_b with T is comparatively flat.

In the quantum ring, the inner edge atoms and the outer edge atoms do not belong to the same sublattice, and the value of their spin correlation is likely to be negative. When we calculate the edge magnetic susceptibility of the quantum ring, the spin correlations of the inner and outer boundaries are separately calculated and then these values are subsequently added. Thus, the edge magnetism is not directly impacted by the spin correlation between the inner and outer edges.

As illustrated in Figs. 6(b) and 6(d), χ_z with respect to temperature is fitted under the on-site interactions $U = 3.0|t|$ and $U = 1.6|t|$. The Curie-Weiss law is satisfied by the edge magnetic susceptibilities of bilayer TGQDs and bilayer TGQRs, and there is a strong edge ferromagnetic correlation. This reveals that the zigzag edge of the bilayer TGQD has a slightly greater Curie constant (C) than the zigzag edge of the bilayer TGQR. The former is $U = 3.0|t|$, $C = 0.75$ and

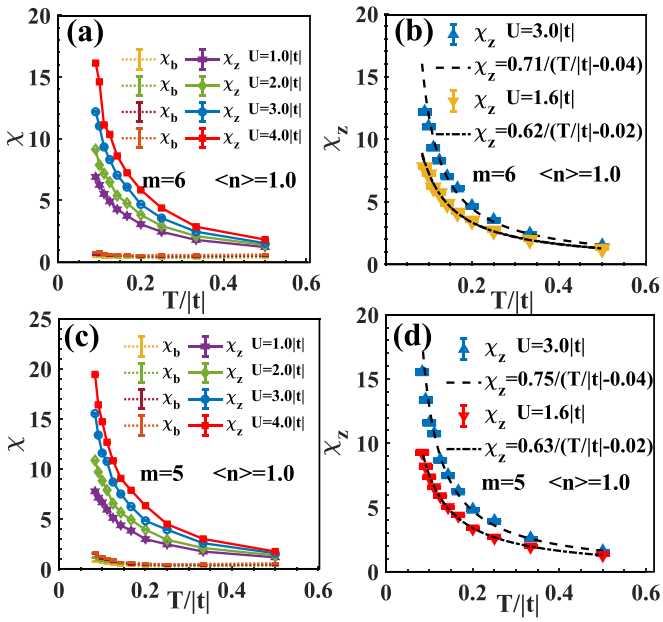

FIG. 6. m in the tag represents the number of hexagons contained by the edge of (a) bilayer TGQR/(c) bilayer TGQD. The χ_z (solid line) and χ_b (dotted line) of (a) a bilayer TGQR with 114 sites and (c) a bilayer TGQD with 92 sites at $\langle n\rangle = 1.0$ with $U = 1.0 \sim 4.0|t|$. The χ_z of (b) a bilayer TGQR and (d) a bilayer TGQD with $U = 1.6|t|$ (positive triangle marker) and $3.0|t|$ (inverted triangle marker), the dashed line represents the fitting of Curie's law when $U = 3.0|t|$, while the dotted line represents the fitting when $U = 1.6|t|$.

$U = 1.6|t|$, $C = 0.63$. The latter is $U = 3.0|t|$, $C = 0.71$ and $U = 1.6|t|$, $C = 0.62$, and their critical temperatures for the ferromagnetic-paramagnetic phase transition are similar. The reason might be that the bilayer TGQD already has significant edge ferromagnetism, and the ring structure adds more ferromagnetic boundaries while the original edge ferromagnetism remains the same. Because relatively few zigzag edge atoms have already demonstrated a very strong ferromagnetic correlation, as shown in Fig. 7, χ_z and χ_b of the bilayer TGQD and bilayer TGQR is nearly unchanged with the increase of structure size.

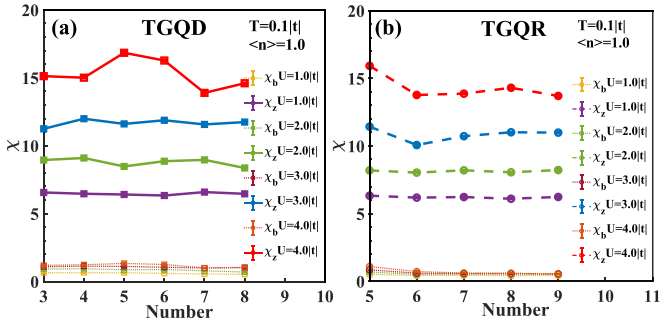

FIG. 7. The χ_z and χ_b of bilayer TGQD (square marker) and bilayer TGQR (circle marker) of different size as shown in the subgraphs with different U. "Number" represents the number of hexagons contained by the edge of bilayer TGQD or bilayer TGQR.

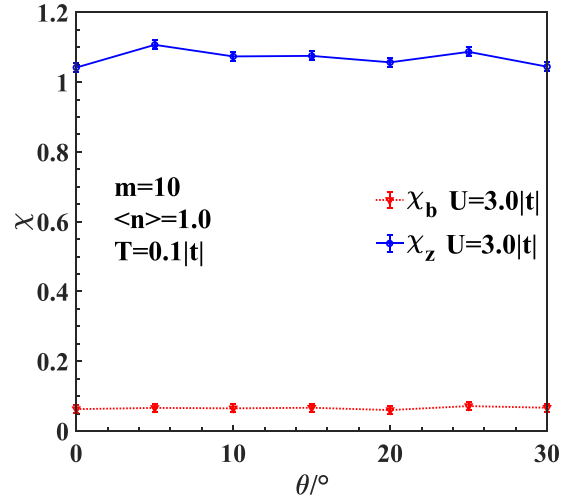

FIG. 8. The ferromagnetic susceptibility of a bilayer TGQR in various twist angles.

IV. SUMMARY OF RESULTS

In summary, based on the Hubbard model, we computed the robust edge ferromagnetism of the TGQD-like system using DQMC. The TGQD-like structure, which includes TGQRs, bilayer TGQDs, and bilayer TGQRs, was chosen because it reflects the zigzag border condition among the various quantum dot (ring) shapes. Our results show that temperature has a significant impact on the edge magnetic susceptibility of such systems. We use the Curie-Weiss law to fit the TGQD-like system, which shows that it exhibits robust edge ferromagnetic behavior. One way to improve the edge magnetic susceptibility and increase the Curie temperature is to increase on-site Hubbard interactions U. The application of TGQD-like systems in spintronics may benefit from robust edge ferromagnetic behavior.

ACKNOWLEDGMENTS

This work was supported by Beijing Natural Science Foundation (No. 1242022), NSFC (No. 11974049), and Guangxi Key Laboratory of Precision Navigation Technology and Application, Guilin University of Electronic Technology (No. DH202322). The numerical simulations in this work were performed at the HSCC of Beijing Normal University.

APPENDIX

When simulating the physics of many-body interaction systems, the computational cost grows exponentially with the size of the lattice. Therefore, our simulations are confined to a relatively small system and may provide some enlightening results for describing truncated small lattices.

We provide the results for different angles below to validate our study for the lattice size we simulated. We can see that the magnetic susceptibility hardly changes with the twist angle in Fig. 8.

We next discuss different NNN hopping parameters in the TGQRs in Fig. 9. Our results show that ferromagnetism is not affected by NNN hopping at $t' = 0.0|t|, 0.1|t|, 0.3|t|$, which

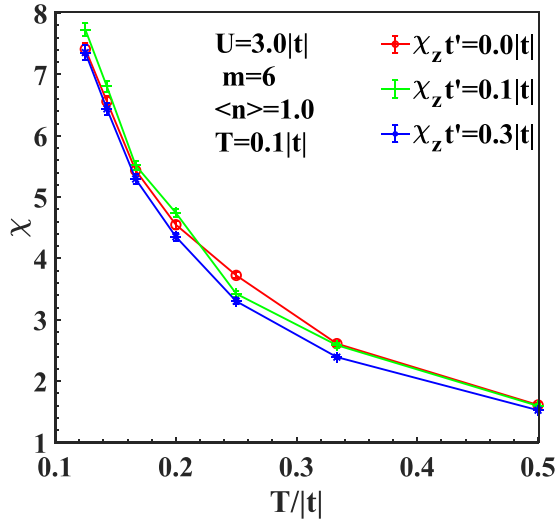

FIG. 9. The ferromagnetic susceptibility as a function of temperature at the zigzag edge when NNN hopping is introduced.

is consistent with the analytic expression for tight-binding dispersion [57]. Therefore, our simulations show that this system has robust edge ferromagnetism even when considering intralayer NNN hopping.

In order to further investigate the effect of the on-site interaction U on the Curie temperature, we plot the reciprocal of χ as depicted below in Fig. 10. The figures exhibit a linear correlation between $1/\chi$ and temperature T, which corresponds to the Curie-Weiss behavior $1/\chi = (T - T_c)/A$. Therefore, we extrapolate $1/\chi$ to zero temperature by using linear fitting. If the system possesses a finite T_c, its intercept should be negative. Figure 10 shows that the on-site interaction U enhances the ferromagnetism and the absolute value of the intercept becomes larger with increasing U both in TGQR and TGQD.

We further add an additional potential at the zigzag edges of the system, to investigate a realistic system in which zigzag edges are decorated by adding atoms. To accomplish this, we change the chemical potential of the edge atoms from $-2|t|$ to $2|t|$ and adjust the bulk chemical potential to maintain half-filling, as shown in Fig. 11(a). Our simulation results show that the magnetic susceptibility χ_z has a maximum value when the chemical potential of the edge atoms is 0, and χ_b remains almost stable in this range. Additionally,

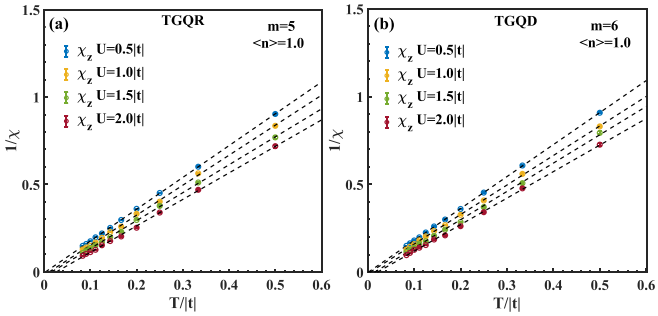

FIG. 10. Linear fitting of the inverse of χ_z of TGQR and TGQD versus temperature at half-filling state.

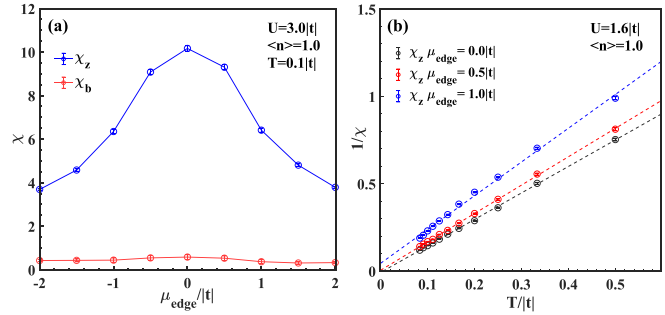

FIG. 11. (a) Linear fitting of the inverse of χ_z of TGQR versus temperature at different edge chemical potentials and the whole system maintains half-filling state. (b) Ferromagnetic susceptibility χ_z and χ_b of TGQR at 114 sites for different boundary chemical potentials at $\langle n \rangle = 1.0$, and $\beta = 1/T$ represents the reciprocal of the temperature.

Fig. 11(b) indicates that as the absolute value of the edge potential changes from 0.0 to $0.5|t|$ at half-filling state, the edge ferromagnetism of the system gradually disappears. It is interesting that even a tiny U is enough to make the edge ferromagnetic at half filling. If including a nonzero edge potential, this phenomenon disappears and one needs finite U for magnetism to appear where edge states getting nonflat dispersion. This behavior could be expected from Stoner criterion. Thus, our results provide important guidance for understanding the physics of TGQD-like system edge doping experiments.

To inspect the validity of inverse temperature β chosen in the main text, we refer to Fig. 12. Because the bilayer TGQR is the most complex structure among those discussed in our work, we consider this material as an example worth further discussion. The values of the correlation functions S_b^{AFM} tend to stabilize with the increase of β at $U = 1.0|t| \sim 3.0|t|$, where $S_b^{\mathrm{AFM}} = \frac{1}{N_t}\langle[\sum_{li}(\widehat{S}^z_{lai} - \widehat{S}^z_{lbi})]^2\rangle$ [19], and $\widehat{S}^z_{lai}$ ($\widehat{S}^z_{lbi}$) is the z component spin operator on A (B) sublattice of layer l. So the value of temperature used in our paper is sufficiently large.

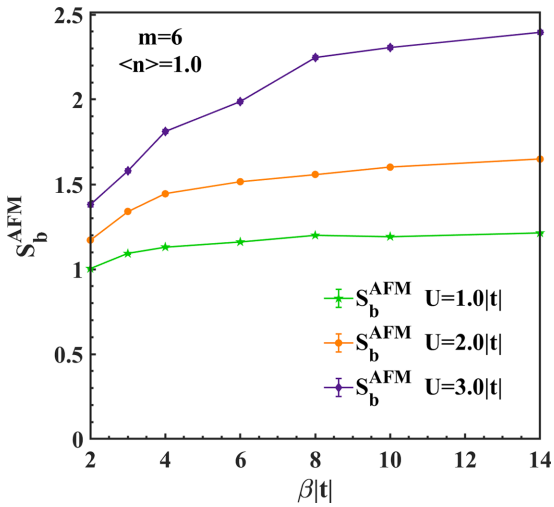

FIG. 12. The antiferromagnetic correlation of bilayer TGQR as a function of $\beta = 1/T$ for different $U = 1.0|t| \sim 3.0|t|$.

[1] K. S. Novoselov, A. K. Geim, S. V. Morozov, D. Jiang, Y. Zhang, S. V. Dubonos, I. V. Grigorieva, and A. A. Firsov, Electric field effect in atomically thin carbon films, Science **306**, 666 (2004).

[2] A. H. Castro Neto, F. Guinea, N. M. R. Peres, K. S. Novoselov, and A. K. Geim, The electronic properties of graphene, Rev. Mod. Phys. **81**, 109 (2009).

[3] M. Long, Z. Zhan, P. A. Pantaleón, J. Á. Silva-Guillén, F. Guinea, and S. Yuan, Electronic properties of twisted bilayer graphene suspended and encapsulated with hexagonal boron nitride, Phys. Rev. B **107**, 115140 (2023).

[4] X. Fan, W. Huang, T. Ma, L.-G. Wang, and H.-Q. Lin, Electronic band gaps and transport properties in periodically alternating mono- and bi-layer graphene superlattices, Europhys. Lett. **112**, 58003 (2015).

[5] L. Di Mauro Villari and A. Principi, Optotwistronics of bilayer graphene, Phys. Rev. B **106**, 035401 (2022).

[6] F. J. G. de Abajo, Graphene nanophotonics, Science **339**, 917 (2013).

[7] M. Wang, M. Huang, D. Luo, Y. Li, M. Choe, W. K. Seong, M. Kim, S. Jin, M. Wang, S. Chatterjee *et al.*, Single-crystal, large-area, fold-free monolayer graphene, Nature (London) **596**, 519 (2021).

[8] J. Son, S. Lee, S. J. Kim, B. C. Park, H.-K. Lee, S. Kim, J. H. Kim, B. H. Hong, and J. Hong, Hydrogenated monolayer graphene with reversible and tunable wide band gap and its field-effect transistor, Nat. Commun. **7**, 13261 (2016).

[9] C. Shen, Y. Chu, Q. Wu, N. Li, S. Wang, Y. Zhao, J. Tang, J. Liu, J. Tian, K. Watanabe *et al.*, Correlated states in twisted double bilayer graphene, Nat. Phys. **16**, 520 (2020).

[10] P. A. Pantaleón, A. Jimeno-Pozo, H. Sainz-Cruz, V. T. Phong, T. Cea, and F. Guinea, Superconductivity and correlated phases in non-twisted bilayer and trilayer graphene, Nat. Rev. Phys. **3**, 304 (2023).

[11] A. Nimbalkar and H. Kim, Opportunities and challenges in twisted bilayer graphene: A review, Nano-Micro Letters **12**, 126 (2020).

[12] J. Yi-Ru, C. Yan-Bang, X. Le-De, Y. Wei, and Z. Guang-Yu, From magic angle twisted bilayer graphene to moire superlattice quantum simulator, Acta Phys. Sin. **70**, 118101 (2021).

[13] S. Latil and L. Henrard, Charge carriers in few-layer graphene films, Phys. Rev. Lett. **97**, 036803 (2006).

[14] H. Murata, Y. Nakajima, N. Saitoh, N. Yoshizawa, T. Suemasu, and K. Toko, High-electrical-conductivity multilayer graphene formed by layer exchange with controlled thickness and interlayer, Sci. Rep. **9**, 4068 (2019).

[15] C. Huang, T. M. R. Wolf, W. Qin, N. Wei, I. V. Blinov, and A. H. MacDonald, Spin and orbital metallic magnetism in rhombohedral trilayer graphene, Phys. Rev. B **107**, L121405 (2023).

[16] J. M. B. Lopes dos Santos, N. M. R. Peres, and A. H. Castro Neto, Graphene bilayer with a twist: Electronic structure, Phys. Rev. Lett. **99**, 256802 (2007).

[17] Y. Cao, V. Fatemi, S. Fang, K. Watanabe, T. Taniguchi, E. Kaxiras, and P. Jarillo-Herrero, Unconventional superconductivity in magic-angle graphene superlattices, Nature (London) **556**, 43 (2018).

[18] X. Lu, P. Stepanov, W. Yang, M. Xie, M. A. Aamir, I. Das, C. Urgell, K. Watanabe, T. Taniguchi, G. Zhang *et al.*, Superconductors, orbital magnets and correlated states in magic-angle bilayer graphene, Nature (London) **574**, 653 (2019).

[19] T. Huang, L. Zhang, and T. Ma, Antiferromagnetically ordered mott insulator and $d + id$ superconductivity in twisted bilayer graphene: A quantum Monte Carlo study, Sci. Bull. **64**, 310 (2019).

[20] M. Alimohammadian and B. Sohrabi, Observation of magnetic domains in graphene magnetized by controlling temperature, strain and magnetic field, Sci. Rep. **10**, 21325 (2020).

[21] J. H. Pixley and E. Y. Andrei, Ferromagnetism in magic-angle graphene, Science **365**, 543 (2019).

[22] O. V. Yazyev and M. I. Katsnelson, Magnetic correlations at graphene edges: Basis for novel spintronics devices, Phys. Rev. Lett. **100**, 047209 (2008).

[23] K. Nakada, M. Fujita, G. Dresselhaus, and M. S. Dresselhaus, Edge state in graphene ribbons: Nanometer size effect and edge shape dependence, Phys. Rev. B **54**, 17954 (1996).

[24] H. X. Zhang, Y. X. Gao, and Z. J. Ding, Ferromagnetism in magic-angle twisted bilayer graphene: A Monte Carlo study, arXiv:2206.14432.

[25] A. L. Sharpe, E. J. Fox, A. W. Barnard, J. Finney, K. Watanabe, T. Taniguchi, M. A. Kastner, and D. Goldhaber-Gordon, Emergent ferromagnetism near three-quarters filling in twisted bilayer graphene, Science **365**, 605 (2019).

[26] G. Yang, S. Xu, W. Zhang, T. Ma, and C. Wu, Room-temperature magnetism on the zigzag edges of phosphorene nanoribbons, Phys. Rev. B **94**, 075106 (2016).

[27] P. Ruffieux, S. Wang, B. Yang, C. Sánchez-Sánchez, J. Liu, T. Dienel, L. Talirz, P. Shinde, C. A. Pignedoli, D. Passerone *et al.*, On-surface synthesis of graphene nanoribbons with zigzag edge topology, Nature (London) **531**, 489 (2016).

[28] R. E. Blackwell, F. Zhao, E. Brooks, J. Zhu, I. Piskun, S. Wang, A. Delgado, Y.-L. Lee, S. G. Louie, and F. R. Fischer, Spin splitting of dopant edge state in magnetic zigzag graphene nanoribbons, Nature (London) **600**, 647 (2021).

[29] Y. Sun, Y. Zheng, H. Pan, J. Chen, W. Zhang, L. Fu, K. Zhang, N. Tang, and Y. Du, Magnetism of graphene quantum dots, npj Quantum Mater. **2**, 5 (2017).

[30] K. E. Çakmak, A. Altıntaş, and A. D. Güçlü, Effects of random atomic disorder on the magnetic stability of graphene nanoribbons with zigzag edges, Phys. Rev. B **98**, 115428 (2018).

[31] K. Tada, T. Hashimoto, J. Haruyama, H. Yang, and M. Chshiev, Spontaneous spin polarization and spin pumping effect on edges of graphene antidot lattices, Physica Status Solidi B **249**, 2491 (2012).

[32] K. Tada, N. Kosugi, K. Sakuramoto, T. Hashimoto, K. Takeuchi, Y. Yagi, J. Haruyama, H. Yang, and M. Chshiev, Electron-spin-based phenomena arising from pore edges of graphene nanomeshes, J. Supercond. Novel Magn. **26**, 1037 (2013).

[33] S. Li, L. Tian, L. Shi, L. Wen, and T. Ma, Ferromagnetic properties in low-doped zigzag graphene nanoribbons, J. Phys.: Condens. Matter **28**, 086001 (2016).

[34] Z.-qiang Bao, J.-wen Ding, and J. Qi, Complex landau levels and related transport properties in the strained zigzag graphene nanoribbons, Phys. Rev. B **107**, 125411 (2023).

[35] *Graphene Nanoribbons*, edited by Luis Brey, Pierre Seneor, and Antonio Tejeda (IOP Publishing, Bristol, UK, 2019).

[36] A. L. Rakhmanov, A. V. Rozhkov, and A. O. Sboychakov, Magic radius of an *aa*-stacked bilayer graphene quantum dot, Phys. Rev. B **105**, 235415 (2022).

[37] W. Hu, Y. Huang, X. Qin, L. Lin, E. Kan, X. Li, C. Yang, and J. Yang, Room-temperature magnetism and tunable energy

gaps in edge-passivated zigzag graphene quantum dots, npj 2D Mater. Appl. **3**, 17 (2019).
[38] R. Das, N. Dhar, A. Bandyopadhyay, and D. Jana, Size dependent magnetic and optical properties in diamond shaped graphene quantum dots: A DFT study, J. Phys. Chem. Solids **99**, 34 (2016).
[39] W. L. Wang, S. Meng, and E. Kaxiras, Graphene nanoflakes with large spin, Nano Lett. **8**, 241 (2008).
[40] J. Hrivnák and L. Motlochová, On electron propagation in triangular graphene quantum dots, J. Phys. A: Math. Theor. **55**, 125201 (2022).
[41] M. Mirzakhani, H. C. Park, F. M. Peeters, and D. R. da Costa, Magnetism in twisted triangular bilayer graphene quantum dots, arXiv:2304.06228.
[42] P. Potasz, A. D. Güçlü, O. Voznyy, J. A. Folk, and P. Hawrylak, Electronic and magnetic properties of triangular graphene quantum rings, Phys. Rev. B **83**, 174441 (2011).
[43] D. A. Bahamon, A. L. C. Pereira, and P. A. Schulz, Inner and outer edge states in graphene rings: A numerical investigation, Phys. Rev. B **79**, 125414 (2009).
[44] M. Mirzakhani, D. R. da Costa, and F. M. Peeters, Isolated and hybrid bilayer graphene quantum rings, Phys. Rev. B **105**, 115430 (2022).
[45] M. Zarenia, A. Chaves, G. A. Farias, and F. M. Peeters, Energy levels of triangular and hexagonal graphene quantum dots: A comparative study between the tight-binding and dirac equation approach, Phys. Rev. B **84**, 245403 (2011).
[46] J. Fernández-Rossier and J. J. Palacios, Magnetism in graphene nanoislands, Phys. Rev. Lett. **99**, 177204 (2007).
[47] A. Tiutiunnyk, D. Laroze, J. D. Correa, and M. E. Mora-Ramos, Electronic and magnetic properties of stacked graphene quantum dots, Diam. Relat. Mater. **131**, 109550 (2023).
[48] E. H. Lieb, Two theorems on the Hubbard model, Phys. Rev. Lett. **62**, 1201 (1989).
[49] N. Pavliček, A. Mistry, Z. Majzik, N. Moll, G. Meyer, D. J. Fox, and L. Gross, Synthesis and characterization of triangulene, Nat. Nanotechnol. **12**, 308 (2017).
[50] S. Mishra, D. Beyer, K. Eimre, J. Liu, R. Berger, O. Gröning, C. A. Pignedoli, K. Müllen, R. Fasel, X. Feng, and P. Ruffieux, Synthesis and characterization of π-extended triangulene, J. Am. Chem. Soc. **141**, 10621 (2019).
[51] J. Su, M. Telychko, P. Hu, G. Macam, P. Mutombo, H. Zhang, Y. Bao, F. Cheng, Z.-Q. Huang, Z. Qiu, S. J. R. Tan, H. Lin, P. Jelínek, F.-C. Chuang, J. Wu, and J. Lu, Atomically precise bottom-up synthesis of-extended [5]triangulene, Sci. Adv. **5**, eaav7717 (2019).
[52] S.-Yu Li and L. He, Recent progresses of quantum confinement in graphene quantum dots, Front. Phys. **17**, 33201 (2022).
[53] M. Mirzakhani, F. M. Peeters, and M. Zarenia, Circular quantum dots in twisted bilayer graphene, Phys. Rev. B **101**, 075413 (2020).
[54] M. Eich, F. Herman, R. Pisoni, H. Overweg, A. Kurzmann, Y. Lee, P. Rickhaus, K. Watanabe, T. Taniguchi, M. Sigrist, T. Ihn, and K. Ensslin, Spin and valley states in gate-defined bilayer graphene quantum dots, Phys. Rev. X **8**, 031023 (2018).
[55] D. R. da Costa, M. Zarenia, A. Chaves, J. M. Pereira, G. A. Farias, and F. M. Peeters, Hexagonal-shaped monolayer-bilayer quantum disks in graphene: A tight-binding approach, Phys. Rev. B **94**, 035415 (2016).
[56] Z. Ge, F. Joucken, E. Quezada, D. R. Da Costa, J. Davenport, B. Giraldo, T. Taniguchi, K. Watanabe, N. P. Kobayashi, T. Low *et al.*, Visualization and manipulation of bilayer graphene quantum dots with broken rotational symmetry and nontrivial topology, Nano Lett. **20**, 8682 (2020).
[57] S. Reich, J. Maultzsch, C. Thomsen, and P. Ordejón, Tight-binding description of graphene, Phys. Rev. B **66**, 035412 (2002).
[58] E. Y. Andrei and A. H. MacDonald, Graphene bilayers with a twist, Nat. Mater. **19**, 1265 (2020).
[59] S.-Y. Li, K.-Q. Liu, L.-J. Yin, W.-X. Wang, W. Yan, X.-Q. Yang, J.-K. Yang, H. Liu, H. Jiang, and L. He, Splitting of Van Hove singularities in slightly twisted bilayer graphene, Phys. Rev. B **96**, 155416 (2017).
[60] G. Trambly de Laissardière, D. Mayou, and L. Magaud, Localization of dirac electrons in rotated graphene bilayers, Nano Lett. **10**, 804808 (2010).
[61] P. Moon and M. Koshino, Optical absorption in twisted bilayer graphene, Phys. Rev. B **87**, 205404 (2013).
[62] R. Bistritzer and A. Macdonald, Moire bands in twisted double-layer graphene, Proc. Nat. Acad. Sci. USA **108**, 12233 (2010).
[63] S. R. White, D. J. Scalapino, R. L. Sugar, E. Y. Loh, J. E. Gubernatis, and R. T. Scalettar, Numerical study of the two-dimensional Hubbard model, Phys. Rev. B **40**, 506 (1989).
[64] R. Blankenbecler, D. J. Scalapino, and R. L. Sugar, Monte Carlo calculations of coupled boson-fermion systems. I, Phys. Rev. D **24**, 2278 (1981).
[65] I. F. Herbut, Interactions and phase transitions on graphene's honeycomb lattice, Phys. Rev. Lett. **97**, 146401 (2006).
[66] D. Baeriswyl, D. K. Campbell, and S. Mazumdar, Correlations and defect energies, Phys. Rev. Lett. **56**, 1509 (1986).
[67] S. Cheng, J. Yu, T. Ma, and N. M. R. Peres, Strain-induced edge magnetism at the zigzag edge of a graphene quantum dot, Phys. Rev. B **91**, 075410 (2015).
[68] M. Schüler, M. Rösner, T. O. Wehling, A. I. Lichtenstein, and M. I. Katsnelson, Optimal Hubbard models for materials with nonlocal coulomb interactions: Graphene, silicene, and benzene, Phys. Rev. Lett. **111**, 036601 (2013).